Journal of Solid State Chemistry 249 (2017) 154–159

Contents lists available at ScienceDirect

Journal of Solid State Chemistry

journal homepage: www.elsevier.com/locate/jssc

The impact of chemical doping on the magnetic state of the Sr_2YRuO_6 double perovskite

Paula Kayser[a], Ben Ranjbar[a], Brendan J. Kennedy[a,*], Maxim Avdeev[b]

[a] School of Chemistry, The University of Sydney, Sydney, NSW 2006, Australia
[b] Australian Nuclear Science and Technology Organisation, Lucas Heights, NSW 2234, Australia

ARTICLE INFO

Keywords:
Ruthenium perovskite
Crystal and magnetic structure
Rietveld refinement
Neutron diffraction

ABSTRACT

The impact of chemical doping of the type $Sr_{2-x}A_xYRuO_6$ (A=Ca, Ba) on the low temperature magnetic properties of Sr_2YRuO_6, probed using variable temperature magnetic susceptibility, neutron diffraction and heat capacity measurements, are described. Specific-heat measurements of un-doped Sr_2YRuO_6 reveal two features at ~26 and ~30 K. Neutron scattering measurements at these temperatures are consistent with a change from a 2D ordered state to the 3D type 1 AFM state. Magnetic and structural studies of a number of doped oxides are described that highlight the unique low temperature behavior of Sr_2YRuO_6 and demonstrate that doping destabilizes the intermediate 2D ordered state.

1. Introduction

Double perovskites $A_2BB'O_6$ with 1:1 rock salt like ordering can be described as having two interpenetrating face-centered-cubic sublattices, where the B and B' cations are located at the corners of an edge-sharing tetrahedral network [1]. In the particular case where a non-magnetic cation is located at one of the octahedral B-sites and a magnetic ion is on the other, long range nearest-neighbor antiferromagnetic interactions cannot be simultaneously established. Consequently, such a cation arrangement offers an excellent opportunity for the design of novel geometrically frustrated magnetic materials [2]. Such systems have been recently attracting considerable attention since they display a wide variety of exotic magnetic states including spin-liquids, spin-glasses and spin-ice [3,4]. The large number of competing ground states in geometrically frustrated magnets tends to destabilize magnetic ordering and may lead to remarkable correlated states at low temperatures.

The crystal symmetry of the double perovskite Sr_2YRuO_6, reported in 1984 by Battle and Macklin [5], is monoclinic (space group $P2_1/n$), with the unit-cell parameters related with the ideal simple perovskite cell as $a\approx\sqrt{2}a_0$, $b\approx\sqrt{2}a_0$ and $c\approx2a_0$, $\beta\approx90°$, where a_0 is the edge of the primitive cubic ABO_3 perovskite. This superstructure is due to ordering of the Ru^{+5} (d^3) and Y^{3+}(diamagnetic) cations over the two octahedral sites in combination with distortion of the oxygen sublattice. The latter can be described in terms of cooperative tilting of the three-dimensional network of corner sharing BO_6 octahedra [6,7]. In recent years, Sr_2YRuO_6 has aroused considerable interest aimed at explaining its anomalous magnetic behavior [8–10]. These include negative values of the zero-field-cooled susceptibility curves, the presence of two low temperature transitions in the heat capacity measurements and the reduced value of ΔS_{mag}. To date a complete understanding of the magnetic properties of Sr_2YRuO_6 remains unclear.

Two recent studies by Granado et al. [11] and Bernardo et al. [12] have used neutron scattering to address our understanding of the unusual properties of Sr_2YRuO_6, however they proposed very different explanations. Granado concluded that the two features observed in the heat capacity arise due to changes from a 2D ordered state to the 3D type 1 AFM state whereas Bernardo *et al.* proposed a different K_2NiF_4-type magnetic structure and argued the two transitions are a consequence of spin reorientation of the net FM moment associated with a non-collinear spin configuration.

In the present contribution we firstly study the anomalous low temperature behavior of the perovskite Sr_2YRuO_6 by means of low temperature neutron powder diffraction, coupled with bulk susceptibility and heat capacity measurements. Having established the crystal and magnetic structures of undoped Sr_2YRuO_6 the influence of chemical doping in oxides of the type $Sr_{2-x}A_xYRuO_6$ (A=Ca, Ba) was investigated. The doped oxides were chosen to maintain the monoclinic $P2_1/n$ structure of the parent. Analysis shows that both larger and smaller cations destabilize the intermediate 2D ordered state seen in Sr_2YRuO_6.

2. Experimental

Approximately 10 g samples of Sr_2YRuO_6, $Sr_{1.5}Ca_{0.5}YRuO_6$, $Sr_{1.5}Ba_{0.5}YRuO_6$ and $Sr_{1.75}Ba_{0.25}YRuO_6$ were synthesized by solid state

* Corresponding author.

http://dx.doi.org/10.1016/j.jssc.2017.03.001
Received 22 November 2016; Received in revised form 27 February 2017; Accepted 1 March 2017
Available online 02 March 2017

methods. Stoichiometric amounts of $SrCO_3$, $BaCO_3$, $CaCO_3$, Y_2O_3 and Ru powder were grounded together in an agate mortar, placed in alumina crucibles and heated as follows: 12 h at 650 °C and 12 h at 850 °C with intermediate regrinding. After mixing again the powders were pressed into 20 mm pellets and heated in air at 1050 °C for 24 h, 1200 °C for 72 h and finally at 1400 °C for 72 h. The magnetic structure of Sr_2YRuO_6 at 5 K and its thermal evolution were determined from Neutron Powder Diffraction (NPD) data in the temperature range 5–75 K measured on the Echidna diffractometer [13] at ANSTO's Opal facility using neutrons of wavelength 2.44 Å. The NPD for the doped samples were measured at low temperatures using the same setup.

DC magnetic susceptibility data were collected under zero field cooled (ZFC) and field cooled (FC) conditions, using a Quantum Design Physical Properties Measurement System (PPMS), over the temperature range 4–300 K in a field of 1000 Oe using the vibrating sample magnetometer technique. Heat capacity measurements were collected from 4–100 K on the same platform using a thermal relaxation method. In order to estimate the magnetic heat capacity C_{mag} (T), the phononic and electronic contributions were subtracted from the total measured heat capacity by fitting a polynomial equation, $C_{Lat} = \sum_{n=0,1,2..5}^{n} A_n T^n$, for temperature intervals outside the region of interest.

3. Results and discussion

Fig. 1 shows the thermal evolution of the NPD patterns for Sr_2YRuO_6 in the range from 5 to 75 K. At 30 K the presence of additional low-angle reflections associated with the magnetic contribution to the scattering is observed, which is consistent with the onset of long-range antiferromagnetic ordering evident in the bulk susceptibility measurements. Although no long-range ordering magnetic peaks are observed above of 30 K, diffuse magnetic scattering persisted up to 75 K. Similar diffuse scattering was also observed in the recent study of Granado et al. [11], and has also been found in other double perovskites including Ba_2YRuO_6 [14] and La_2LiOsO_6 [15].

The crystal and magnetic structures below T_N were determined from the Rietveld analyses [16] of the NPD data, using the computer program Fullprof [17]. The plot of the observed and calculated profiles, including both the crystallographic and magnetic phases, is shown in Fig. 2a. Table 1 includes the most important refined parameters. All of the magnetic peaks were indexed with the propagation vector k=(000), thus the magnetic unit cell coincides with the chemical one. The propagation vector has been calculated using K_SEARCH in FullProf and the subsequent determination of the magnetic structure was accompanied using BasIrep as implemented in Fullprof [17]. Among the possible magnetic modes compatible with the space-group symmetry and this propagation vector, the best agreement with the experimental data was obtained for the magnetic structure where the Ru_1(0,0,0) and Ru_2(½,½,½) spins are magnetically coupled as $m_{1x}=-m_{2x}$, $m_{1y}=m_{2y}=0$, $m_{1z}=-m_{2z}$. The refined components of the magnetic moment along the crystallographic axes at 5 K are m_x=2.16(2) μ_B and m_z=−0.4(1) μ_B, and the net moment is 2.19(2) μ_B, which is consistent with the previously reported values of 1.85(10) μ_B [5] and 1.96 μ_B [11]. The moment reduction with respect to the theoretical magnetic moment, 3μ_B (S=3/2) per Ru^{5+}, is likely due to covalency effects in the Ru–O bonds [5]. We also tested the k=½, ½, 0 propagation vector with the moments in the *ab*-plane, however this did not reproduce the magnetic intensity ratios and gave an unacceptably high R_{mag}~32%. Interestingly, the k=½, ½, 0 model with the moment along the *c*-axis produces very similar magnetic intensities to those of k=0,0,0 (R_{mag}=8.00%) with the moments in the *ab*-plane but the R_{mag} is still slightly higher (10%).

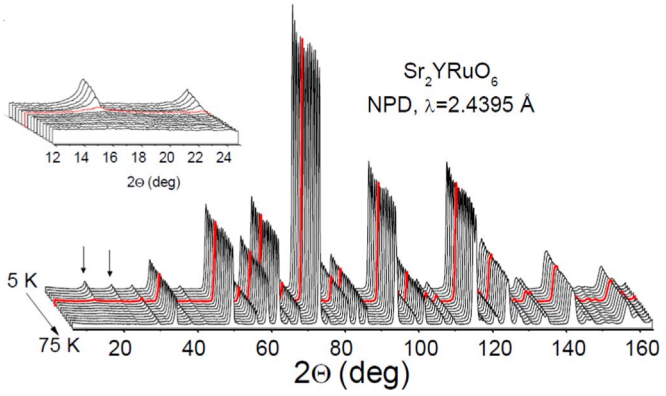

Fig. 1. Thermal evolution of the NPD patterns of Sr_2YRuO_6, acquired with λ=2.44 Å in the temperature interval 5 < T < 75K. The pattern collected at 30 K is red colored to indicate the origin of additional peaks due to the coherent magnetic scattering. The inset shows a magnified portion in the 12 < 2Θ < 25 region.

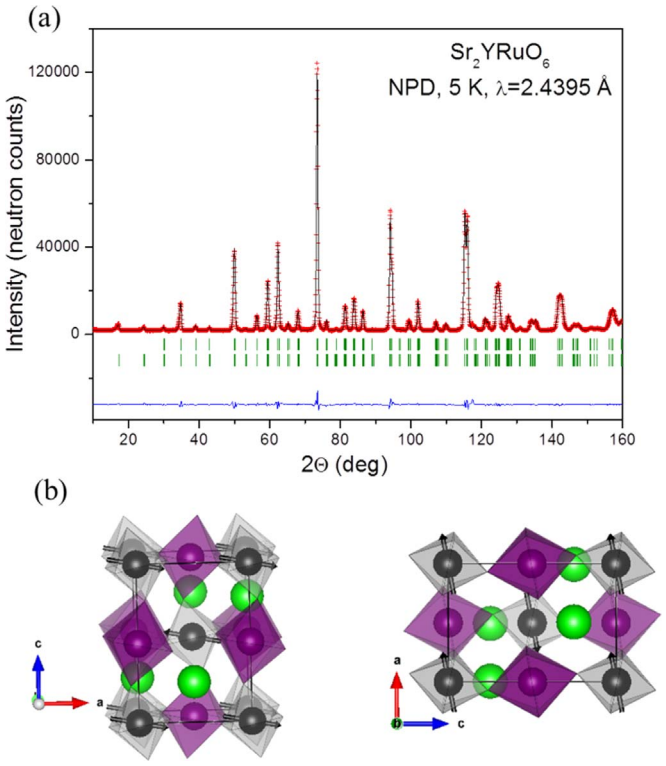

Fig. 2. (a) Observed (crosses), calculated (solid line) and difference (bottom) NPD Rietveld profiles for Sr_2YRuO_6 at 5 K collected at Echidna diffractometer (ANSTO). The upper and lower series of Bragg reflections correspond to the nuclear and magnetic phase respectively. (b) Schematic view of the magnetic structure of Sr_2YRuO_6 below T_{N2}.

As shown in Fig. 2b, the magnetic structure consists of ferromagnetic (001) layers of Ru^{5+} moments coupled antiferromagnetically along [001], characteristic of a type-I Anti-Ferromagnetic Structure (AFM) structure, as originally identified by Battle and Macklin [5]. This model is different from that described recently by Bernardo et al. [12], a point we will return to below.

In order to correlate the NPD results with those obtained from heat capacity and magnetic susceptibility measurements, the temperature dependence of the spin orientation near the magnetic ordering temperatures was examined, Figs. 3 and 4. The magnetic susceptibilities of the samples was previously reported under both field cooled (FC) and zero-field cooled (ZFC) conditions in Ref 24. The data in the paramagnetic region were analysed using a linear Curie–Weiss fit from which the Weiss constant and the effective moment per formula unit were determined (Table 1-Ref 24). The negative Weiss temperature, θ=−273.54 K, indicates that the predominant magnetic interactions are antiferromagnetic. The observed effective magnetic moment (3.73μB)

Table 1
Unit-cell, atomic positions, thermal parameters and selected interatomic bond distances (Å) and angles (°) for $Sr_{2-x}A_xYRuO_6$ refined in space group $P2_1/n$ (no. 14), against powder neutron diffraction data.

	$Ca_{0.5}Sr_{1.5}YRuO_6$	$Ca_{0.5}Sr_{1.5}YRuO_6$	Sr_2YRuO_6	$Ba_{0.25}Sr_{1.75}YRuO_6$	$Ba_{0.5}Sr_{1.5}YRuO_6$
T (K)	20	3	5	3	3
Space Group	$P2_1/n$	$P2_1/n$	$P2_1/n$	$P2_1n$	$P2_1/n$
a (Å)	5.7150(3)	5.71518(17)	5.75664(9)	5.78208(14)	5.80593(16)
b (Å)	5.7658(3)	5.76592(18)	5.7812(1)	5.78731(17)	5.79542(14)
c (Å)	8.1073(4)	8.10730(20)	8.1489(1)	8.17160(20)	8.19080(20)
β(°)	90.3604(10)	90.3594(6)	90.2898(5)	90.2686(6)	90.2406(10)
Vol ($Å^3$)	267.1428(37)	267.1568(37)	271.196(8)	273.4407(36)	275.6(36)
A x	0.4937(9)	0.4936(6)	0.4937(5)	0.4929(8)	0.4923(8)
y	0.0348(4)	0.0347(3)	0.03120(2)	0.0247(3)	0.0192(5)
z	0.2518(7)	0.2514(4)	0.2512(4)	0.2510(6)	0.2541(7)
B_{iso} ($Å^2$)	0.50(10)	0.54(6)	0.23(2)	0.41(3)	0.49(4)
Y					
B_{iso} ($Å^2$)	0.69(14)	1.03(9)	0.20(4)	0.59(5)	0.26(5)
Ru					
B_{iso} ($Å^2$)	0.66(3)	0.63(8)	0.23(2)	0.41(3)	0.49(4)
O1 x	0.5768(9)	0.5769(5)	0.5706(4)	0.5645(7)	0.5573(8)
y	0.4792(6)	0.4798(4)	0.4843(4)	0.4870(6)	0.4915(7)
z	0.2647(5)	0.2645(3)	0.2668(3)	0.2659(3)	0.2648(4)
B_{iso} ($Å^2$)	0.96(11)	1.05(6)	0.32(6)	0.62(9)	0.29(13)
O2 x	0.1953(8)	0.1948(5)	0.1961(5)	0.2052(8)	0.2060(8)
y	0.2744(7)	0.2735(4)	0.2687(4)	0.2633(7)	0.2607(8)
z	0.0411(6)	0.0407(4)	0.0362(4)	0.0314(5)	0.0283(6)
B_{iso} ($Å^2$)	0.92(12)	1.09(6)	0.30(6)	1.28(13)	0.81(12)
O3 x	0.7259(6)	0.7247(4)	0.7323(3)	0.7336(6)	0.7399(7)
y	0.1999(7)	0.1995(4)	0.1987(4)	0.2008(7)	0.2090(9)
z	0.9654(7)	0.9652(4)	0.9641(5)	0.9683(6)	0.9694(7)
B_{iso} ($Å^2$)	0.77(13)	0.92(7)	0.27(8)	−0.13(11)	0.88(15)
Ru-O1(Å)	1.964(4)	1.965(2)	1.947(2)	1.9522(25)	1.957(3)
Ru-O2 (Å)	1.963(4)	1.957(3)	1.942(3)	1.9475(43)	1.940(5)
Ru-O3 (Å)	1.964(4)	1.968(2)	1.943(2)	1.9459(37)	1.951(5)
Y-O1 (Å)	2.191(4)	2.1894(24)	2.212(2)	2.2042(25)	2.193(3)
Y-O2 (Å)	2.201(4)	2.2055(27)	2.223(3)	2.2027(44)	2.212(5)
Y-O3 (Å)	2.178(4)	2.1761(23)	2.216(2)	2.2120(39)	2.202(5)
B-O_{avg} (Å)	2.0768	2.0768	2.0805	2.0774	2.0758
Y-O1-Ru (°)	154.62(16)	154.64(10)	156.8(1)	158.82(10)	161.29(13)
Y-O2-Ru (°)	154.17(17)	154.35(10)	156.7(1)	160.49(17)	162.02(18)
Y-O3-Ru (°)	157.06(15)	156.75(9)	157.43(8)	159.28(15)	161.86(18)
Y-O-Ru_{avg} (°)	155.28	155.25	156.98	159.53	161.72
μ_x (BM)	1.24(8)	1.93(4)	2.16(2)	2.09(2)	2.11(3)
μ_y (BM)	1.1(1)	1.36(8)	0	1.22(6)	1.36(7)
μ_z (BM)	0	−0.92(9)	−0.4(1)	0	0
$R_{nuclear}$	2.26	2.43	1.25	2.20	2.47
R_{mag}	18.8	25.5	8.0	15.4	18.5

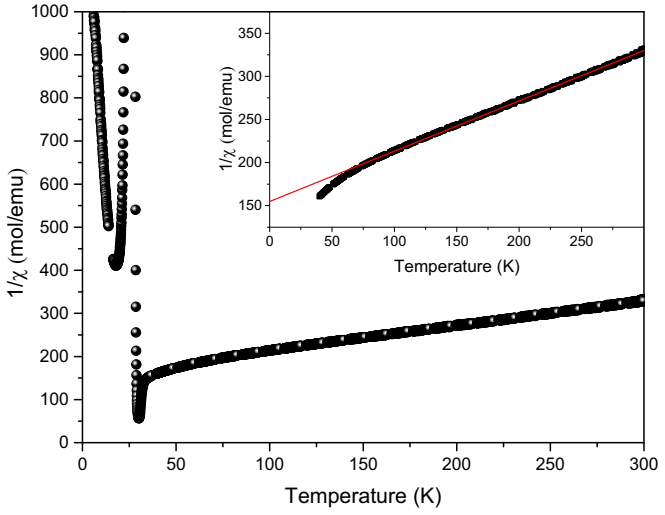

Fig. 3. Temperature dependence of the inverse magnetic susceptibility for Sr_2YRuO_6 measured under ZFC conditions. The inset shows the Curie-Weiss fit to the high temperature (50–300 K) region and highlights the curvature at low temperatures.

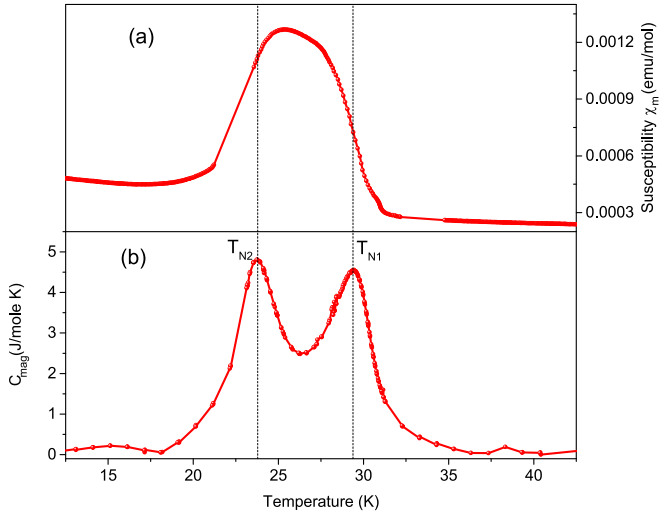

Fig. 4. Low temperature (a) the ZFC magnetization (χ_m) and (b) magnetic heat capacity C_{mag} for Sr_2YRuO_6. The magnetic heat capacity was corrected for the lattice contribution estimated by fitting a polynomial function outside the area of interest $15K < T\ and\ T > 45K$.

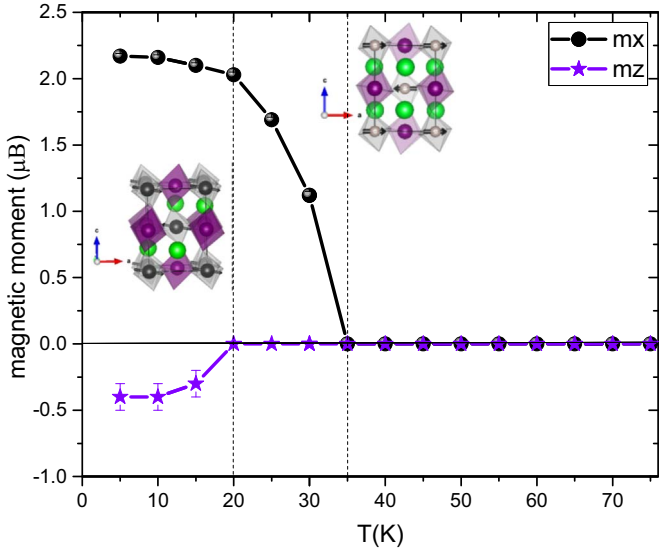

Fig. 5. Thermal evolution of the *x* and *z* components of the magnetic moment. The right inset drawing represents a collinear spin arrangement while the left one shows a canted antiferromagnetic structure.

is in good agreement with the spin-only value for the d^3 Ru^V ion (3.87μB) and is appreciably larger than the ordered moment refined from the NPD data of 2.19(2) μB.

As previously reported [18] two transitions are evident in the heat capacity measurements at T_{N1}~28 K and T_{N2}~24 K (Fig. 4). That both of these are magnetic is evident from the susceptibility curve. The thermal evolution of the magnetic parameters refined against the NPD data is illustrated in Fig. 5. The first notable feature of this figure is the short-range magnetic correlations between nearest neighbor Ru^{5+} cations above the magnetic order temperature, which agrees with previous studies, that have observed 2D short magnetic interactions persisting above T_{N2} [11]. This is the origin of the diffuse scattering described above. On cooling, the material undergoes a transition to a long-range magnetically ordered state which is manifested by the appearance of sharp diffraction peaks in the data set collected at 30 K. This is consistent with the feature in the heat capacity data (Fig. 4) observed at T_{N1}. The magnetic structure below T_{N1} can be described as a collinear antiferromagnetic structure with the magnetic moments aligned along the *a*-axis. The second anomaly in the heat capacity data at T_{N2} ~24 K corresponds to the appearance of a non-zero *z* component of the magnetic moment, although the magnetic structure overall remains AFM (Fig. 5 inset). Singh and Tomy [8] have proposed, based on isothermal magnetization measurements, that the long range magnetic order starts near T_{N1} with a ferromagnetic component as a consequence of canting of the antiferromagnetically ordered Ru moments due to Dzyaloshinsky-Moriya interactions. At T_{N2} a second ferromagnetic component appears which cancels with the first, [8] indicating the spin arrangement cannot be strictly collinear as suggested by the neutron data. Symmetry allows ferromagnetic coupling of m_{1y}=m_{2y}, and although the *y* component of the magnetic moment is zero at both T_{N1} and T_{N2}, weak ferromagnetism, has been observed in studies using a single crystal of Sr_2YRuO_6 [19]. The ferromagnetic component of 0.05 μB/Ru reported in [19] is much lower than detection limit of neutron powder diffraction.

It is critical to note that the second transition at T_{N2} corresponds to spin reorientation rather than a change in the magnetic structure type and critically no additional reflections are observed in our NPD data. In this regard our results are different from those of Bernardo et al. [12] who reported an additional reflection near Q=0.86 $Å^{-1}$ that they fitted using a propagation vector k=(½ ½ 0). The model proposed by Bernardo et al. was described as of a K_2NiF_4 type spin structure, although such a structure has a k=(000) propagation vector. We explain the discrepancy by the fact that the magnetic sublattice is virtually cubic (within 0.04 Å tolerance) in Sr_2YRuO_6 and it is not easy to distinguish k=(000) and (½ ½ 0). To confirm our hypothesis we tested the K_2NiF_4 model with the k=(½ ½ 0) and the moments in the *ab*-plane and found that, whilst it indexes the additional magnetic reflections in a LeBail type fitting, this model gives incorrect magnetic intensity ratios and significantly higher R_{mag} (8.00 vs. 11.62%). We therefore confirm that the type-I AFM magnetic structure is established at T_{N1}, in agreement with the earlier work of Battle [5] and Granado et al. [11] and there is no evidence is for a change in the magnetic propagation vector between T_{N1} and T_{N2}.

Diffuse magnetic scattering persists to at least 75 K indicating the presence of short-range spin correlations and consequently we conclude that the onset of magnetic order in Sr_2YRuO_6 is, as proposed by Granado [11] gradual, transitioning from a short range ordered state at high temperatures, via a partially ordered state at T_{N1} to the fully ordered type 1 structure at T_{N2}. This change in spin-spin correlations is manifested in the appearance of two features in the heat-capacity. A similar gradual transition has been observed in cubic Ba_2YRuO_6 [20], where 2D correlations are important below T_{N2}, that is in the partially ordered state. A combination of weak anisotropy and/or weak next nearest neighbor interactions is responsible for the observed long range magnetic order [21]. Despite their different crystal symmetry both Sr_2YRuO_6 and Ba_2YRuO_6 display an intermediate ordered spin state suggesting that the 2D magnetic correlations in the double perovskite three-dimensional lattice is a consequence of the inherent geometric frustration associated with the FCC Ru network. The deviation from linear Curie–Weiss, evident below around 60 K in Fig. 3, may be correlated with the distribution of magnetic moments shown in Fig. 5, which form the angular magnetic structure. This consistent with the postulates of Granado et al. [11] and Bernardo et al. [12].

Although not commonly observed there is now some evidence that the formation of the long range ordered AFM ground state in double perovskites involves a partially ordered intermediate state. The cause of this unusual behavior is unclear although it is possible that magnetic frustration associated with the lattice motif, rather than spin reorientation, is important [10]. The estimated value for the magnetic entropy for Sr_2YRuO_6 (ΔS_{mag}~1.6 $Jmol^{-1}$ K^{-1}) is similar to that reported previously [8,18,22] and the absolute value of this can be understood since the magnetic ground state occurs via an intermediate configuration since the long-range spin structure below T_{N1} is not a completely ordered magnetic state.

In addition to providing direct evidence for a change in the magnetic structure at T_{N2} the structural refinements extend the earlier work of Granado et al. [11] by providing precise unit cell parameters, proving the opportunity to examine the possibility of coupling between the spin and lattice. The thermal evolution of the structural parameters obtained here shows that the transition to the magnetic state does not involve any unusual structural change. Indeed as illustrated for the monoclinic angle (Fig. 6) which increases upon cooling reaching a plateau near 50 K due to saturation effects, the temperature dependence of the unit cell parameters suggests the absence of appreciable magnetostriction. The change in the monoclinic angle is similar to that observed in non-magnetic double perovskites such as $Ba_2Bi^{III}Bi^{V}O_6$ at low temperatures [23]. Evidently there is little coupling between the spin and the lattice in Sr_2YRuO_6.

Turning now to the influence of chemical doping, low temperature heat capacity measurements of some chemically doped oxides of the type $Sr_{2-x}Ba_xYRuO_6$ reveal that the separation of the two features is sensitive to the precise occupancy of the *A*-type cation site, Fig. 7. The present results for Ba doping are similar to that described for Ca doping by Bernardo et al. [18], evidently both Ca and Ba doping suppressing the formation of the intermediate partially ordered state, demonstrating that this is not simply correlated with the Y-O-Ru angles which are expected to increase as the average size of the *A*-site cation increases [24,25]. Whilst somewhat surprising, this is consistent with

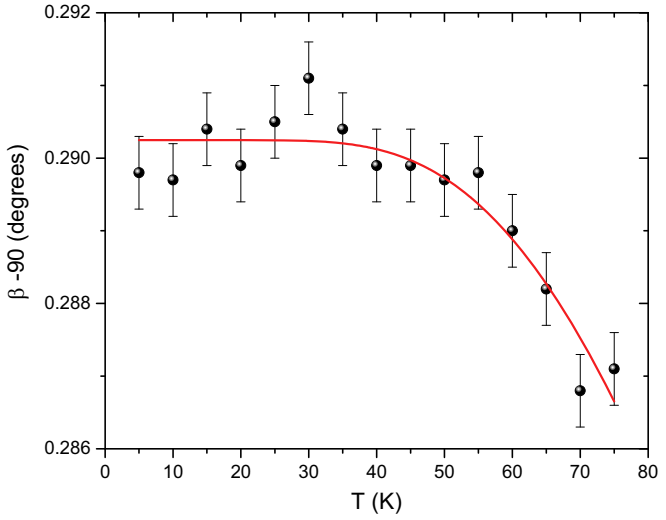

Fig. 6. Thermal evolution of the monoclinic angle as (β−90). The solid red line corresponds to the linear least squares fit to to an expression of the type $\beta - 90° \propto A + B*C*\coth(C/T)$.

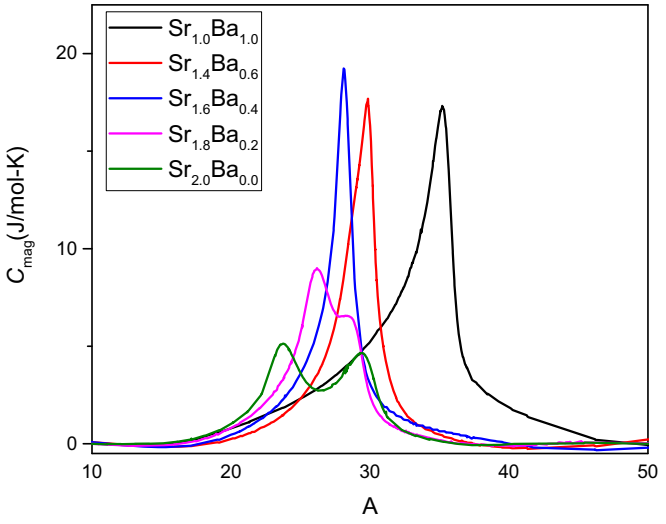

Fig. 7. Temperature dependence of the heat capacity for samples in the series $Sr_{2-x}Ba_xYRuO_6$. This figure demonstrates that Ba doping suppresses the formation of the intermediate partially ordered state.

the variable temperature structural studies of undoped Sr_2YRuO_6 described above that show there is little coupling between the spin and the lattice. Given the systematic changes in the separation of the two features in the heat capacity upon doping the impact of chemical pressure on the magnetic structure, introduced by changing the average *A*-site sizes [18,24], was investigated through low temperature neutron diffraction studies of the three oxides; $Sr_{1.5}Ca_{0.5}YRuO_6$, $Sr_{1.5}Ba_{0.5}YRuO_6$ and $Sr_{1.75}Ba_{0.25}YRuO_6$. The results of these studies are summarized in Fig. 8. The structures were refined in space group $P2_1/n$, and selected structural parameters are given in Table 1. In all cases the NPD patterns contained a number of magnetic peaks that could be indexed with the propagation vector k=(000). In each case the magnetic structure is the same as that displayed by Sr_2YRuO_6, consisting ferromagnetic (001) layers of Ru^{5+} moments coupled antiferromagnetically along [001], characteristic of a type-I AFM structure.

The low temperature neutron diffraction measurements confirmed our expectation that as the effective *A*-site size increases, the octahedral tilting diminishes and the Y-O-Ru angle approaches the ideal value of 180°. This improves the orbital overlap between 4*d* Ru and 2*p* O

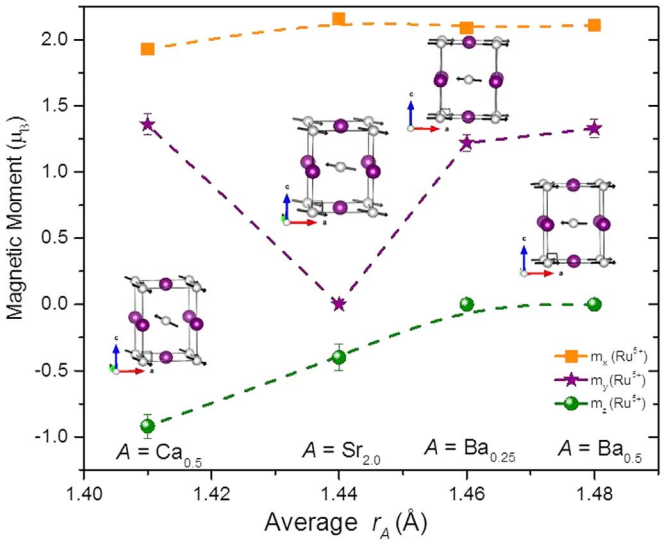

Fig. 8. Variation of m_x, m_y and m_z with the average size of the A-site for oxides of the type $Sr_{2-x}A_xYRuO_6$ deduced from neutron diffraction data measured at 5 K.

orbital, enhancing the superexchange interaction. This leads to an increase in the magnetic ordering temperature from ~24 K in Sr_2YRuO_6 to ~35 K in (SrBa)$YRuO_6$. Conversely reducing the *A*-site cation size increases the magnitude of the octahedral tilting and the average Y-O-Ru angle becomes further removed from 180° (see Table 1). Remarkably either increasing (Ba doping) or decreasing (Ca doping) the effective size of the *A*-site cation introduces an appreciable magnetic moment along the *b*-axis. Whilst the structural parameters and the moments along the *a* and *c*-axis scale with the size of the *A*-site cation, Fig. 8 shows that the *y* component does not, and initially it might be suspected that this is correlated with the appearance of two features in the heat capacity measurements, although since both $Sr_{1.5}Ca_{0.5}YRuO_6$ and $Sr_{1.75}Ba_{0.25}YRuO_6$, like Sr_2YRuO_6, show two peaks in the heat capacity measurements this is not the case.

Fig. 8 reveals that the spin direction in Sr_2YRuO_6 is different from that of its doped analogues. We start by noting that the formation of the intermediate ordered spin state is not a condition for this and re-emphasise that this is not related to the appearance of two low temperature magnetic transitions. Noting that in the type-I AFM magnetic structure the 12 nearest neighbor (NN) interactions involve 4 Ferromagnetic and 8 Antiferromagnetic correlations whilst the next nearest neighbor (NNN) interactions involve 6 Ferromagnetic correlations. In a non-cubic structure these will be sensitive to the precise Ru-O-Y-O-Ru interactions and it appears that the delicate balance between these determines the precise spin orientation in these oxides. Indeed weak ferromagnetism, characterized by large irreversibility in both magnetic susceptibility and isothermal magnetization, has been observed in a single crystal of Sr_2YRuO_6 [19]. Note that because of the essentially cubic metric crystal structure the lattice directions in that work, based on electron diffraction, can be assigned arbitrarily, whereas neutron diffraction is highly sensitive to subtle oxygen displacements, which are what makes the structure monoclinic and allows unique axis assignment.

In summary we have confirmed that the magnetic structure of Sr_2YRuO_6 is, as described previously by Granado et al. a Type 1 antiferromagnet [11]. The appearance of two features in both the heat capacity and magnetic susceptibility measurements is a consequence of a transition from a 2D to 3D ordered structures and not, as postulated by Bernardo et al. due to spin re-orientation [12]. The persistence of diffuse magnetic scattering to well above T_N appears to a common feature in rock-salt ordered double perovskites reflecting the magnetic frustration in these. The temperature dependence of the unit cell parameters in Sr_2YRuO_6 suggests the absence of appreciable magne-

tostriction and this is consistent with studies of a number of doped species of the type $Sr_{2-x}Ba_xYRuO_6$. Disseler et al. have shown that the NN and NNN interactions in Sr_2YRuO_6 are of a similar magnitude and that single ion anisotropy induced by spin-orbit coupling and distortion of the oxygen octahedra around the Ru cations will influence the relative strengths if the superexchange pathways [26]. We postulate that the sensitivity of the low temperature magnetic properties in Sr_2YRuO_6 is a consequence of competition between the in-plane ferromagnetically aligned and out-of-plane AFM aligned Ru pairs and that the relative strength of these evolves with the precise nature of the monoclinic distortion.

Acknowledgments

This work has been supported by the Australian Research Council.

References

[1] T. Aharen, J.E. Greedan, F. Ning, T. Imai, V. Michaelis, S. Kroeker, H.D. Zhou, C.R. Wiebe, L.M.D. Cranswick, Phys. Rev. B 80 (2009) 134423.
[2] J.P. Carlo, J.P. Clancy, K. Fritsch, C.A. Marjerrison, G.E. Granroth, J.E. Greedan, H.A. Dabkowska, B.D. Gaulin, Phys. Rev. B 88 (2013) 024418.
[3] J.E. Greedan, J. Mater. Chem. 11 (2001) 37–53.
[4] A.P. Ramirez, Annu. Rev. Mater. Sci. 24 (1994) 453–480.
[5] P.D. Battle, W.J. Macklin, J. Solid State Chem. 52 (1984) 138–145.
[6] S. Vasala, M. Karppinen, Prog. Solid State Chem. 43 (2015) 1–36.
[7] C.J. Howard, B.J. Kennedy, P.M. Woodward, Acta Crystallogr. Sect. B-Struct. Sci. 59 (2003) 463–471.
[8] R.P. Singh, C.V. Tomy, Phys. Rev. B 78 (2008) 024432.
[9] G. Long, M. DeMarco, D. Coffey, M.K. Toth, M.S. Torikachvili, Phys. Rev. B 87 (2013) 024416.
[10] S. Garcia, L. Ghivelder, Solid State Commun. 179 (2014) 11–15.
[11] E. Granado, J.W. Lynn, R.F. Jardim, M.S. Torikachvili, Phys. Rev. Lett. 110 (2013) 017202.
[12] P.L. Bernardo, L. Ghivelder, H.S. Amorim, J.J. Neumeier, S. Garcia, New J. Phys. 17 (2015) 103007.
[13] K.-D. Liss, B. Hunter, M. Hagen, T. Noakes, S. Kennedy, Physica B-Condens. Matter 385–86 (2006) 1010–1012.
[14] G.J. Nilsen, C.M. Thompson, G. Ehlers, C.A. Marjerrison, J.E. Greedan, Phys. Rev. B 91 (2015) 054415.
[15] C.M. Thompson, C.A. Marjerrison, A.Z. Sharma, C.R. Wiebe, D.D. Maharaj, G. Sala, R. Flacau, A.M. Hallas, Y. Cai, B.D. Gaulin, G.M. Luke, J.E. Greedan, Phys. Rev. B 93 (2016) 014431.
[16] H.M. Rietveld, J. Appl. Crystallogr. 2 (1969) 65.
[17] J. Rodriguez-Carvajal, Physica B 192 (1993) 55–69.
[18] P.L. Bernardo, L. Ghivelder, G.G. Eslava, H.S. Amorim, I. Felner, S. Garcia, J. Solid State Chem. 220 (2014) 270–276.
[19] G. Cao, Y. Xin, C.S. Alexander, J.E. Crow, Phys. Rev. B 63 (2001) 184432.
[20] G.J. Nilsen, C.M. Thompson, G. Ehlers, C.A. Marjerrison, J.E. Greedan, Phys. Rev. B 91 (2015).
[21] E.V. Kuz'min, S.G. Ovchinnikov, D.J. Singh, J. Exp. Theor. Phys. 96 (2003) 1124–1130.
[22] P.L. Bernardo, L. Ghivelder, G.G. Eslava, H.S. Amorim, E.H.C. Sinnecker, I. Felner, J.J. Neumeier, S. Garcia, J. Phys.-Condens. Matter 24 (2012) 486001.
[23] B.J. Kennedy, C.J. Howard, K.S. Knight, Z.M. Zhang, Q.D. Zhou, Acta Crystallogr. Sect. B-Struct. Sci. 62 (2006) 537–546.
[24] B. Ranjbar, A. Pavan, B.J. Kennedy, Z.M. Zhang, Dalton Trans. 44 (2015) 10689–10699.
[25] P.J. Saines, B.J. Kennedy, M.M. Elcombe, J. Solid State Chem. 180 (2007) 401–409.
[26] S.M. Disseler, J.W. Lynn, R.F. Jardim, M.S. Torikachvili, E. Granado, Phys. Rev. B 93 (2016) 140407.